Inelastic electron scattering from excited barium atoms

Rajesh Srivastava
Department of Physics, Indian Institute of Technology—Roorkee, Roorkee 247667, India

A. D. Stauffer
Department of Physics and Astronomy, York University, Toronto, Canada M3J 1P3
(Received 11 January 2005; published 31 May 2005)

We have carried out relativistic distorted-wave calculations for inelastic electron scattering from the $6s5d\ ^{1,3}D_2$ and $6s6p\ ^1P_1$ excited states of barium in the energy range from 20 to 40 eV. Results are presented for the differential cross sections and electron-impact coherence parameters and compared with experimental measurements and other theoretical calculations for these quantities.

DOI: 10.1103/PhysRevA.71.052715 PACS number(s): 34.80.Dp

I. INTRODUCTION

There has been little work, either experimental or theoretical, on electron-induced transitions between excited states of atoms. A notable exception is barium where sufficiently large populations of excited states can be produced by laser irradiation to allow for the measurement of inelastic and superelastic scattering processes from these states. Pioneering work was carried out by Register *et al.* [1] and more recent experiments by Zetner and his co-workers [2–7] have refined and extended these measurements. In addition, unitarized distorted-wave approximation (UDWA) and converged close-coupling (CCC) calculations have been performed for these processes and reported in the references given above. The results reported in these references are differential cross sections (DCSs) for various inelastic and superelastic transitions between excited states induced by electron collisions. In addition, the electron-impact coherence parameters (EICPs) are obtained by interpreting the experiments as the time reversal of electron-collision-induced transitions followed by radiative decay.

The experimental measurements involve laser excitation to the $6s6p\ ^1P_1$ level of barium. Since the laser light is linearly or circularly polarized the excited state is represented as a coherent superposition of magnetic substates. However, if these states are allowed to decay radiatively, the $6s5d\ ^{1,3}D_2$ metastable states are populated and radiation trapping produces incoherent states [5]. There are sufficient numbers of atoms in these metastable states that electron scattering experiments can be performed and cross sections for excitation to higher-lying excited states measured.

Alternatively, electrons can be scattered, either inelastically or superelastically, directly from the $6s6p\ ^1P_1$ states. The resulting cross sections depend on the direction of the laser beam and the plane of polarization (in the case of linearly polarized light) and are denoted as partial differential cross sections (PDCSs) [4]. By varying the laser geometry, the DCS can be obtained from the measured PDCS [5]. As well, the EICP for the time-reversed collision process can also be obtained from the PDCS. In this time-reversed interpretation, the $6s6p\ ^1P_1$ state is always the final excited state which radiates to the ground state [2,3,6,7].

We have previously used the relativistic distorted-wave (RDW) method to calculate electron excitation from the ground state of barium [8,9] and obtained results which were in generally good agreement with experiment and other theoretical work. In this paper we apply the RDW method to the inelastic and superelastic scattering of electrons from excited states of barium in order to compare with the experimental and theoretical results referred to above. This is a test case for the reliability of the RDW method for scattering from excited states.

II. THEORETICAL CONSIDERATIONS

Barium is a sufficiently heavy atom that many of its fine-structure states can be resolved in the scattering experiments listed above. Thus it is important to have a good representation of these target states for the theoretical calculations. We use the GRASP92 program of Parpia *et al.* [10] to produce Dirac-Fock target wave functions. These have the advantage that they represent the fine-structure states directly without the additional recoupling required for the nonrelativistic *LS*-coupled wave functions.

We consider the barium atom to have a closed-shell core $1s^2 2s^2 2\bar{p}^2 2p^4 3s^2 3\bar{p}^2 3p^4 3\bar{d}^4 3d^6 4s^2 4\bar{p}^2 4p^4 4\bar{d}^4 4d^6 5s^2 5\bar{p}^2 5p^4$ in the *j*-*j* coupled notation where, for example, $\bar{p}$ indicates an electron with total angular momentum $j=1/2$ while p is an electron with $j=3/2$ with a similar notation for the other electrons. For the neutral atom there are two valence electrons outside this core. However, the ground and excited states cannot be represented accurately by a single configuration of these two electrons and must be considered in the configuration-interaction form as a linear combination of a number of two-electron configurations.

Our strategy has been to optimize the target wave functions by doing separate calculations for a small group of transitions with specific values of the total angular momentum J of the target states. Thus, for example, we have done one calculation involving the initial states $6s5d\ ^{1,3}D_2$ and the final states $6s6p\ ^3P_2$ and $6p5d\ ^3F_2$ (features 21 and 24 of [4]) and a separate calculation for the same initial states but with final state $6s6p\ ^1P_1$ (features 22 and 23). For those cases where the initial state was $6s6p\ ^1P_1$ we have done a separate

TABLE I. Configurations used in the calculation of the GRASP92 program for the target states when the initial states were $6s5d\ ^{1,3}D_2$. Note that we dropped the $5\bar{d}7s$ and $5d7s$ configurations in the features 40 and 42.

Feature[a]	States	Configurations
	$6s5d\ ^{1,3}D_2$	$5\bar{d}6s, 5d6s, 5\bar{d^2}, 5\bar{d}5d, 5d^2, 5\bar{d}7s, 5d7s, 6\bar{p}6p, 6p^2$
21, 24	$6s6p\ ^3P_2, 6p5d\ ^3F_2$	$6s6p, 5\bar{d}6\bar{p}, 5d6\bar{p}, 5\bar{d}6p, 5d6p$
22, 23	$6s6p\ ^1P_1$	$6s6\bar{p}, 6s6p, 5\bar{d}6\bar{p}, 5\bar{d}6p, 5d6p$
41	$6p5d\ ^3P_2$	$6s6p, 5\bar{d}6\bar{p}, 5d6\bar{p}, 5\bar{d}6p, 5d6p, 6s7p$
40, 42	$6p5d\ ^3P_1, 6s7p\ ^1P_1$[b]	$6s6\bar{p}, 6s6p, 5\bar{d}6\bar{p}, 5\bar{d}6p, 5d6p, 6s7\bar{p}, 6s7p$

[a]Notation of Zetner *et al.* [4].
[b]Moore [11] and Karlsson and Litzén [12] identify this state as $5d6p\ ^1P_1$.

calculation for each transition. Complete details of these calculations are given in Tables I and II.

In Table III we present a comparison of the transition energies and oscillator strengths for those transitions where there are meaningful data for comparison. In particular, we compare our results with experimental values as well as results from the UDWA and CCC calculations. We do not give the energies of the individual levels since in our bound-state calculations the ground configuration was not included. We have reported the gf values for the oscillator strengths (where g is the statistical weight $2J+1$ of the initial level of the transition and f is its oscillator strength) which are independent of the choice for the initial and final states of the transition. In the majority of cases our energies are within 10% of the experimental values but there are several cases where the difference is larger. The CCC calculations give superior agreement in almost all cases while the UDWA accuracy is comparable to the present results. There are less reliable data in the case of oscillator strengths but again the CCC results appear more reliable. In the case of feature 6 our very small value is due to the absence of the ground configuration in the $J=0$ state.

The theoretical development of the RDW method has been given by Zuo *et al.* [13]. Here we calculate the T matrices for the electron excitation of state a to state b,

$$T_{b\leftarrow a} = \langle \Phi_b^{\mathrm{DW}}(N+1) | V-U | \Psi_a^{\mathrm{DW}}(N+1) \rangle \tag{1}$$

where

$$\Phi_b^{\mathrm{DW}}(N+1) = \varphi_b(N) F_b^{\mathrm{DW}-}(N+1) \tag{2}$$

represents the final-state total wave function and

$$\Psi_a^{\mathrm{DW}}(N+1) = A\{\varphi_a(N) F_a^{\mathrm{DW}+}(N+1)\} \tag{3}$$

the total initial wave function. N represents the number of electrons in the target atom (here $N=56$) and V is the Coulomb interaction between the incident electron and the atom. φ_a and φ_b are the configuration-interaction wave functions for the initial and final states of the atom as given in Tables I and II and A is the antisymmetrization operator. $F^{\mathrm{DW}+,-}$ are the outgoing and incoming distorted waves calculated in the presence of the distortion potential U which is taken to be the usual choice of the spherically averaged static potential of the final state φ_b. Since U is a function of the scattered electron only, it does not contribute to the T matrix due to the orthogonality of the atomic wave functions.

TABLE II. Configurations used in the calculation of the GRASP92 program for the target states when the initial state was $6s6p\ ^1P_1$. Note that in the case of features 7 and 12 where the final state was also $^1P_1$, the configurations for the initial and final states were combined.

Feature[a]	States	Configurations
	$6s6p\ ^1P_1$	$6s6\bar{p}, 6s6p, 5\bar{d}6\bar{p}, 5\bar{d}6p, 5d6p$
1	$6p5d\ ^1D_2$	$5\bar{d}6\bar{p}, 5d6\bar{p}, 5\bar{d}6p, 5d6p$
1, 3	$5d^2\ ^1D_2, ^3P_2$	$5\bar{d}6s, 5d6s, 5\bar{d^2}, 5\bar{d}5d, 5d^2, 5\bar{d}7s, 5d7s, 6\bar{p}6p, 6p^2$
6	$6s7s\ ^1S_0$	$6s7s, 6s8s, 6\bar{p^2}, 6p^2, 5\bar{d^2}, 5d^2, 5\bar{d}6\bar{d}, 5d6d$
7	$6s7p\ ^1P_1$	$6s7\bar{p}, 6s7p$
8	$6s6d\ ^1P_2$	$6s6\bar{d}, 6s6d, 5\bar{d^2}, 5\bar{d}5d, 5d^2, 5\bar{d}7s, 5d7s$
12	$6s8p\ ^1P_1$[b]	$6s7\bar{p}, 6s7p, 6s8\bar{p}, 6s8p$
13	$6s8s\ ^3S_1$	$6s8s, 5\bar{d}6\bar{d}, 5\bar{d}6d, 5d6\bar{d}, 5d6d$
19	$6s8d\ ^1D_2$	$6s7\bar{d}, 6s7d, 6s8\bar{d}, 6s8d, 6s9\bar{d}, 6s9d, 5\bar{d^2}, 5\bar{d}5d, 5d^2, 5\bar{d}6\bar{d}, 5\bar{d}6d, 5d6\bar{d}, 5d6d, 6p\bar{6}p, 6p^2$

[a]Notation of [4].
[b]Moore [11] and Karlsson and Litzén [12] identify this state as $6s7p\ ^1P_1$.

TABLE III. Transition energies (eV) and oscillator strengths (gf values). F, feature number; E_{ex}, experimental transition energies [11,12]; gf_{cr}, critically evaluated experimental oscillator strengths [15]. The subscripts RDW, DW, and CCC refer to results from the present calculations, the UDWA results of [4], and the CCC results [16], respectively.

F	Transition states	E_{ex}	E_{RDW}	E_{DW}	E_{CCC}	gf_{cr}	gf_{RDW}	gf_{DW}	gf_{CCC}
1	$6s6p\ ^1P_1$–$5d^2\ ^1D_2$	0.620	1.220	0.732	0.723		0.585		0.204
3	$6s6p\ ^1P_1$–$5d^2\ ^3P_2$	0.726	1.264	0.811	0.860		0.153		0.036
6	$6s6p\ ^1P_1$–$6s7s\ ^1S_0$	1.261	1.200	1.349	1.273		0.00097		0.525
7	$6s6p\ ^1P_1$–$6s7p\ ^1P_1$	1.301	1.206	1.413	1.330	0	0	0	0
8	$6s6p\ ^1P_1$–$6s8d\ ^1P_2$	1.510	1.496	1.734	1.595		1.031		1.245
12	$6s6p\ ^1P_1$–$6s8p\ ^1P_1$	1.796	1.739	2.080		0	0	0	0
13	$6s6p\ ^1P_1$–$6s8s\ ^3S_1$	1.965	1.989	2.071		0.00035	0.00020		
21	$6s5d\ ^3D_2$–$6s6p\ ^3P_2$	0.533	0.473	0.242	0.463		0.0988	0.010	0.045
22	$6s5d\ ^1D_2$–$6s6p\ ^1P_1$	0.826	0.412	0.691	0.834	0.0255	0.0029		0.015
23	$6s5d\ ^3D_2$–$6s6p\ ^1P_1$	1.097	0.714	0.948	1.089		0.00035		0.005
24	$6s5d\ ^1D_2$–$6p5d\ ^3F_2$	1.323	1.123	1.322	1.304		1.260		0.375
40	$6s5d\ ^3D_2$–$6p5d\ ^3P_1$	2.044	1.894	1.957	2.083	0.95	0.647		0.930
41	$6s5d\ ^3D_2$–$6p5d\ ^3P_2$	2.076	1.945	1.823	2.121	0.433	0.641		0.200
42	$6s5d\ ^1D_2$–$6s7p\ ^1P_1$	2.128	1.772	2.104	2.164	0.69	0.174	0.610	0.540

If we specify the total angular momentum and z component of φ_a as J_a, M_a and the spin of the incident electron as μ_a with a similar notation for the final state b then we can write

$$T_{b\leftarrow a} = \langle J_b M_b \mu_b | V | J_a M_a \mu_a \rangle \tag{4}$$

where the quantization axis lies along the direction of the momentum of incident electron (i.e., the collision frame). If we define density matrix elements as

$$\rho_{MM'} = \frac{1}{2} \sum_{\mu_a \mu_b M_a} \langle J_b M \mu_b | V | J_a M_a \mu_a \rangle \langle J_b M' \mu_b | V | J_a M_a \mu_a \rangle^* \tag{5}$$

then, with our normalization of the distorted waves, the differential cross section is given by

$$\sigma = \frac{1}{2J_a + 1} \sum_M \rho_{MM}. \tag{6}$$

Considering the particular case where $J_b = 1$, the PDCS measured by [4] is given by

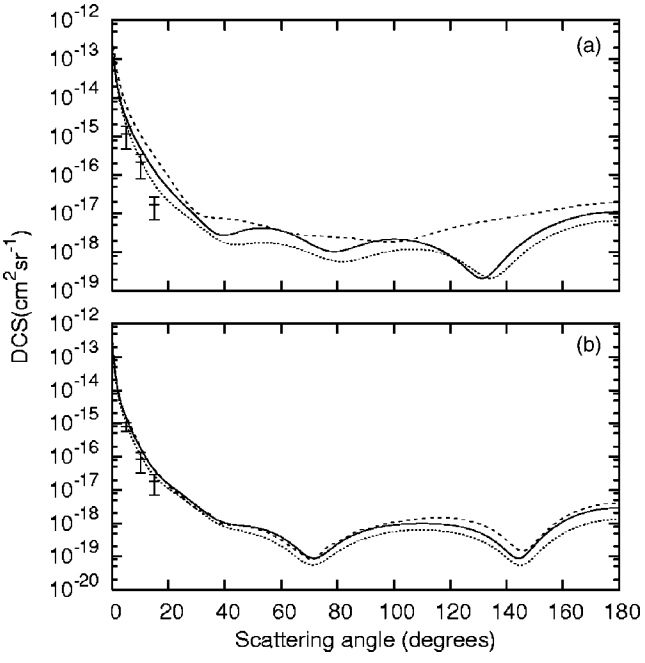

FIG. 1. Differential cross sections for the $6s5d\ ^3D_2$–$6s6p\ ^3P_2$ excitation in barium in units of cm^2/sr at an electron impact energy of (a) 20 and (b) 36.7 eV. The full curves represent the present RDW results. Data from [5] are long-dashed curve, UDWA; short-dashed curve, CCC; + with error bars, experimental measurements.

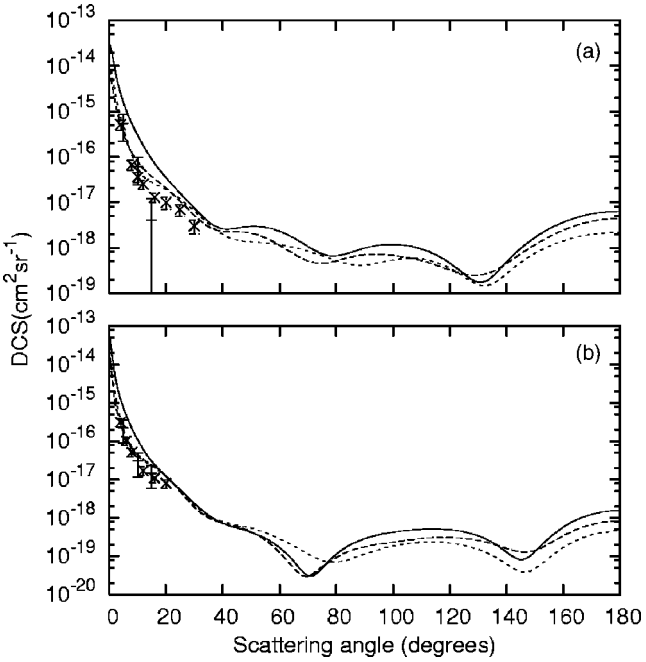

FIG. 2. As for Fig. 1 for the $6s5d\ ^1D_2$–$6s6p\ ^1P_1$ excitation with the addition of the experimental data × with error bars from [6].

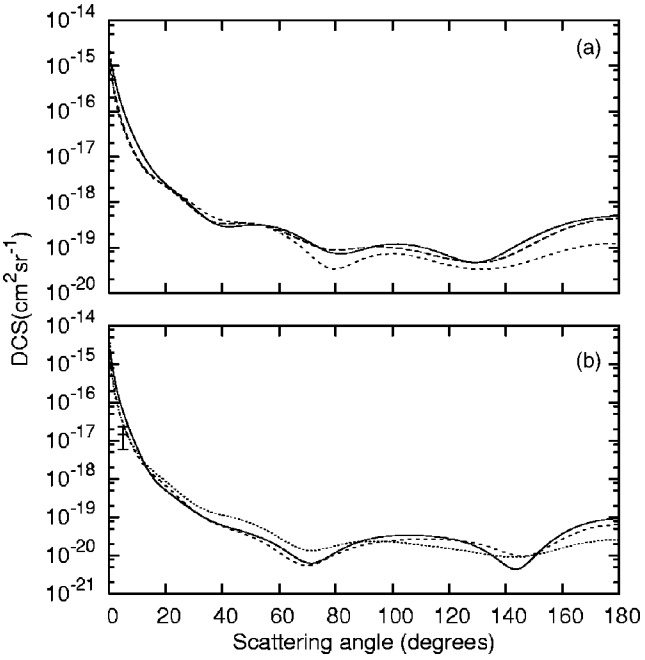

FIG. 3. As for Fig. 1 for the $6s5d\ ^3D_2$–$6s6p\ ^1P_1$ excitation.

$$\sigma^{\mathrm{PDCS}} = \frac{5}{6}\rho_{11} + \frac{1}{6}\rho_{00} + \frac{1}{2}\rho_{-11} - \frac{\sqrt{2}}{3}\mathrm{Re}\,\rho_{01}. \tag{7}$$

Following [6], we define

$$I(\psi) = \frac{1}{2}\{(1 - \cos 2\psi)\rho_{11} + (1 + \cos 2\psi)\rho_{00} - (1 - \cos 2\psi)\rho_{-11} + 2\sqrt{2}\sin 2\psi\,\mathrm{Re}[\rho_{01}]\} \tag{8}$$

and

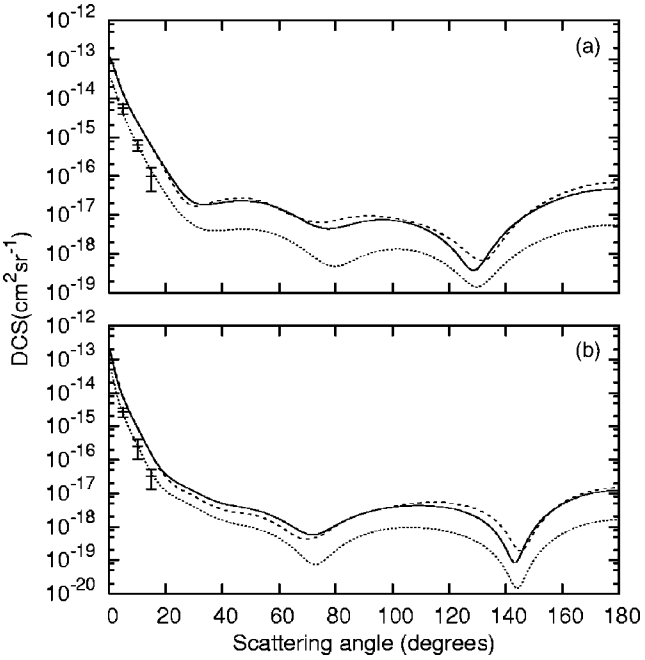

FIG. 4. As for Fig. 1 for the $6s5d\ ^1D_2$–$6p5d\ ^3F_2$ excitation.

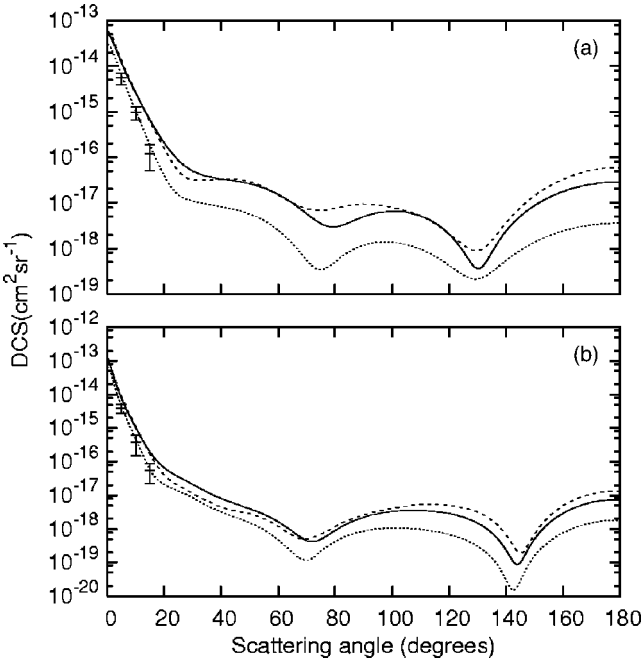

FIG. 5. As for Fig. 1 for the combined $6s5d\ ^3D_2$–$6p5d\ ^3P_1$ and $6s5d\ ^3D_2$–$6p5d\ ^3P_2$ excitations.

$$I(\pm) = \frac{1}{2}\{\rho_{11} + \rho_{00} - \rho_{-11} \pm 2\sqrt{2}\mathrm{Im}[\rho_{01}]\}. \tag{9}$$

Then the Stokes parameters are given by

$$P_1 = \frac{I(0) - I(90)}{I(0) + I(90)}, \tag{10}$$

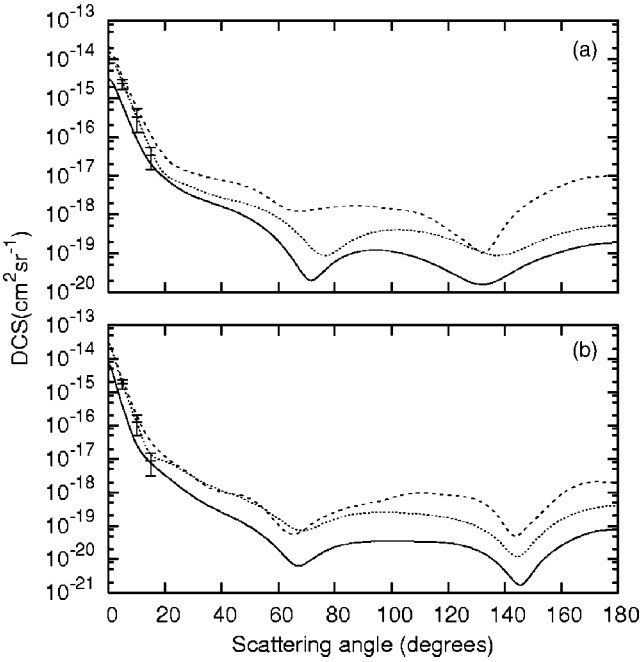

FIG. 6. As for Fig. 1 for the $6s5d\ ^1D_2$–$6s7p\ ^1P_1$ excitation.

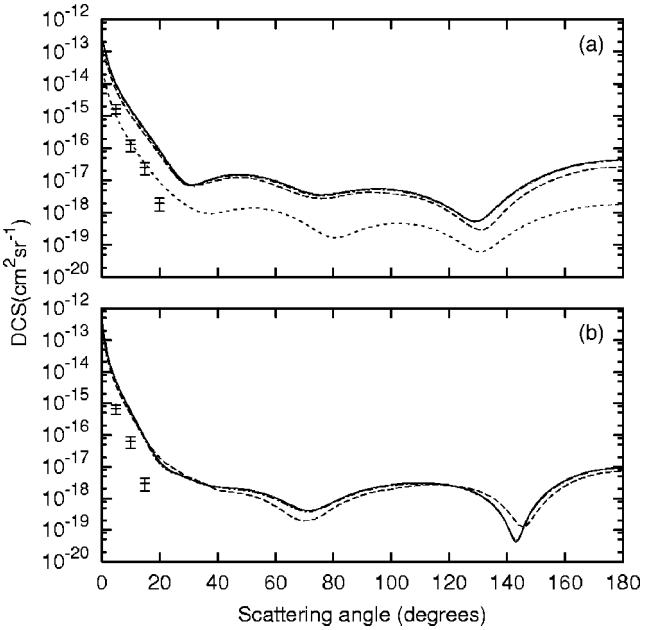

FIG. 7. Differential cross sections for the $6s6p\ ^1P_1$–$5d^2\ ^3P_2$ excitation in barium in units of cm^2/sr at an electron impact energy of (a) 20 and (b) 36.7 eV. The present RDW results for the DCS are shown by the full curve and for the PDCS by the chain curve. The UDWA results from [4] are shown by the long-dashed curve and the CCC results of [16] by the short-dashed curve. The experimental data from [4] are shown as + with error bars.

$$P_2 = \frac{I(45) - I(135)}{I(45) + I(135)}, \tag{11}$$

$$P_3 = \frac{I(+) - I(-)}{I(+) + I(-)}, \tag{12}$$

while the λ parameter is

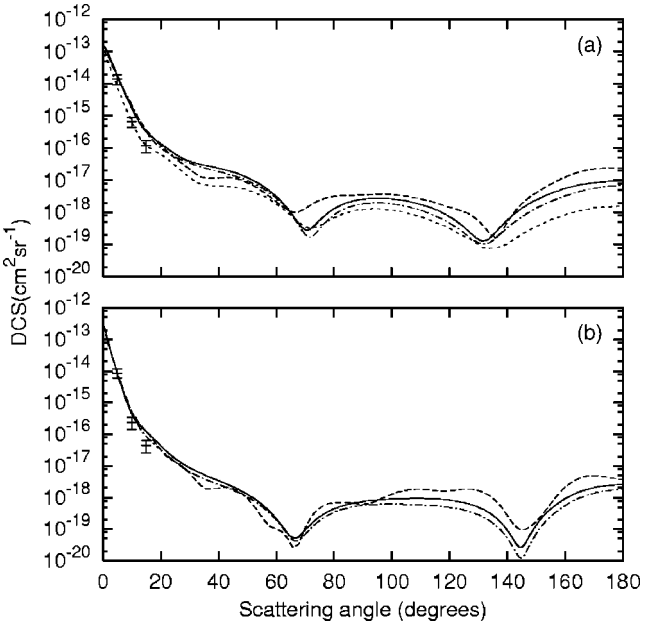

FIG. 8. As for Fig. 7 for the $6s6p\ ^1P_1$–$6s6d\ ^1D_2$ excitation.

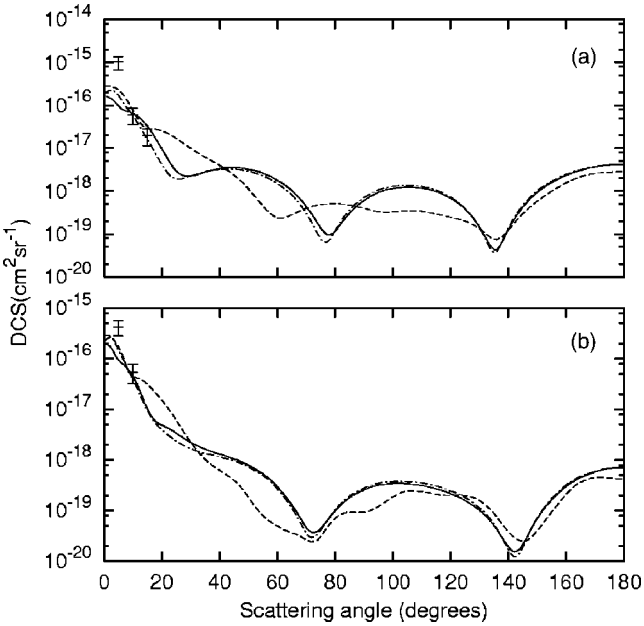

FIG. 9. As for Fig. 7 for the $6s6p\ ^1P_1$–$6s8p\ ^1P_1$ excitation. There are no CCC results for this transition.

$$\lambda = \frac{\rho_{00}}{\rho_{00} + \rho_{11} + \rho_{-1-1}}. \tag{13}$$

III. RESULTS

A. Differential cross sections

Zetner *et al.* [5] have presented differential cross section results, both experimental and theoretical, for excitations from the initial $6s5d\ ^{1,3}D_2$ states to a number of final states. The details for these transitions are given in Table I. In Figs.

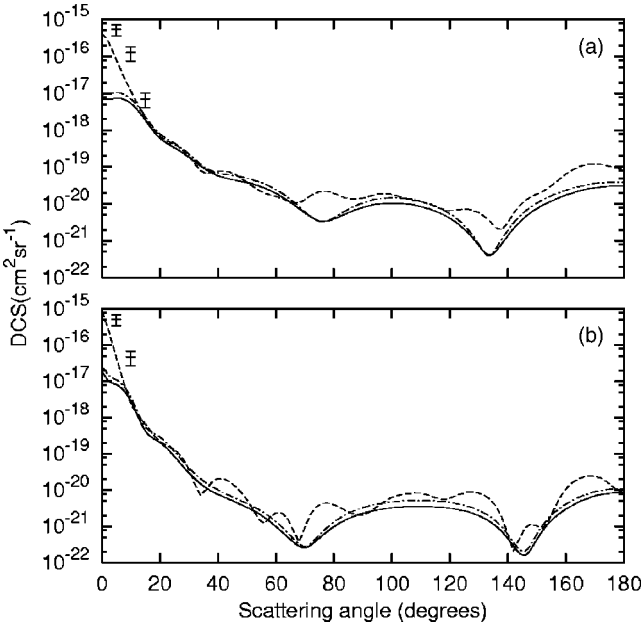

FIG. 10. As for Fig. 9 for the $6s6p\ ^1P_1$–$6s8s\ ^3S_1$ excitation.

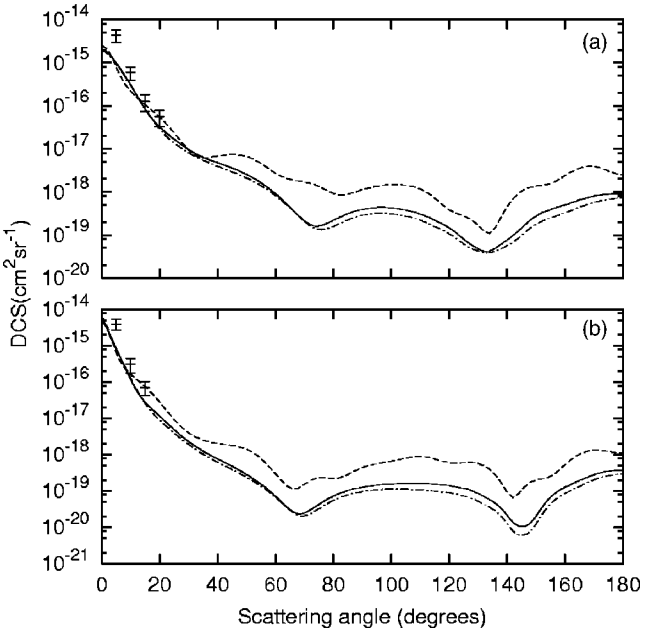

FIG. 11. As for Fig. 9 for the $6s6p\ ^1P_1$–$6s8d\ ^1D_2$ excitation.

1–6 we compare our results for differential cross sections at 20 and 36.7 or 40 eV with those given by Zetner *et al.* [5].

All three theories produce cross sections of similar shape and magnitude although in some cases the UDWA results deviate from the other two for larger scattering angles. Unfortunately, the experimental data are only available for smaller angles limiting the range over which comparisons can be made. In general, the CCC results are in closer agreement with experiment than either the UDWA or present RDW values.

It is somewhat surprising to note that all these cross sections have very similar shapes, which include a sharp forward peak characteristic of an allowed transition. In fact, the shapes are similar to the cross sections for excitation of the ground $6s^2\ ^1S_0$ state to the $6s6p\ ^1P_1$ excited state [8]. The designation given for the initial and final states for the cross sections in Fig. 3, for example, would imply that this is a spin-forbidden transition which would normally have a much smaller and rather flat cross section in the forward direction. However, the notation used for the states arises from *LS* coupling and is not valid for heavy atoms such as barium. As given in Table I, both the initial and final states are linear combinations of a number of configurations in *j-j* coupling some of which lead to allowed transitions. Even if the calculations are carried out in *LS* coupling, it is found that singlets and triplets are mixed so that one cannot depend on the state designation to lead to accurate information about the nature of these transitions.

Zetner *et al.* [4] measured a number of cross sections for inelastic scattering from the $6s6p\ ^1P_1$ excited state to various higher-lying states. The results of UDWA calculations were also included in this paper. Since the $6s6p\ ^1P_1$ state is initially excited by polarized laser light, the state is oriented (i.e., the magnetic substates are unequally populated) and thus what is measured is a "partial differential cross section." For the particular experimental configuration used, the expression for this PDCS is given in Eq. (7). The transitions involved are given in Table II labeled as features 3, 8, 12, 13, and 19. The cross sections for these transitions are shown in Figs. 7–11 for incident electron energies of 20 and 36.7 eV along with the experimental results and the UDWA calculations as well as some unpublished CCC results at 20 eV [16].

Our calculations indicate that the PDCS values are very close to the DCS results. The UDWA calculations give a similar result though their PDCS values are not shown here. For several of these transitions the UDWA calculations exhibit a number of maxima and minima at larger scattering angles which are not predicted by the other theories. Unfortunately these occur beyond the range of the experimental measurements. The excitation of the $6s8p\ ^1P_1$ state shown in Fig. 9 is a forbidden (odd-odd) transition and this is evident by the fact that our RDW cross sections have a much less pronounced peak in the forward direction. There are also significant differences between the PDCSs and DCSs at small scattering angles although these differences are less than the error bars on the experimental results. The UDWA results show the same general pattern of behavior as the RDW ones but with significant differences in magnitude. The excitation of the $6s8s\ ^3S_1$ state is also basically a forbidden transition in our RDW calculation as shown in Fig. 10. Al-

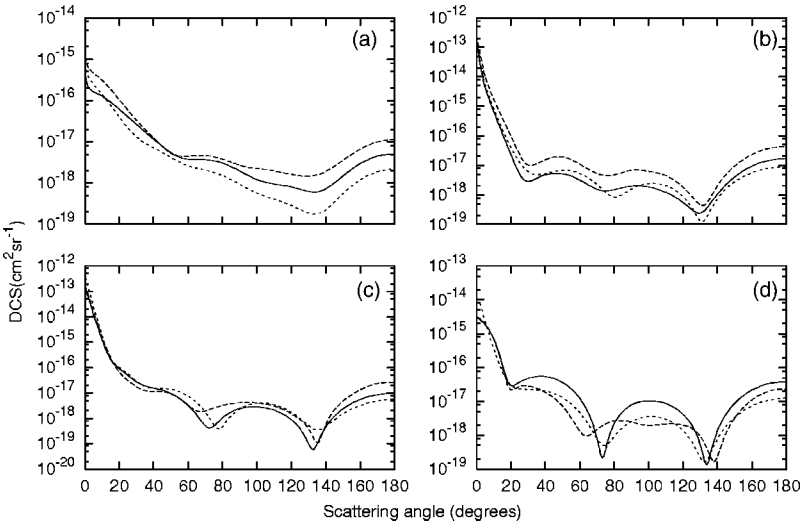

FIG. 12. Differential cross sections for the excitation of the initial $6s6p\ ^1P_1$ state at 20 eV electron-impact energy. The final states are (a) $6p5d\ ^1D_2$; (b) $5d^2\ ^1D_2$; (c) $6s7s\ ^1S_0$; (d) $6s7p\ ^1P_1$. The legend is the same as for Fig. 1 but there are no experimental data.

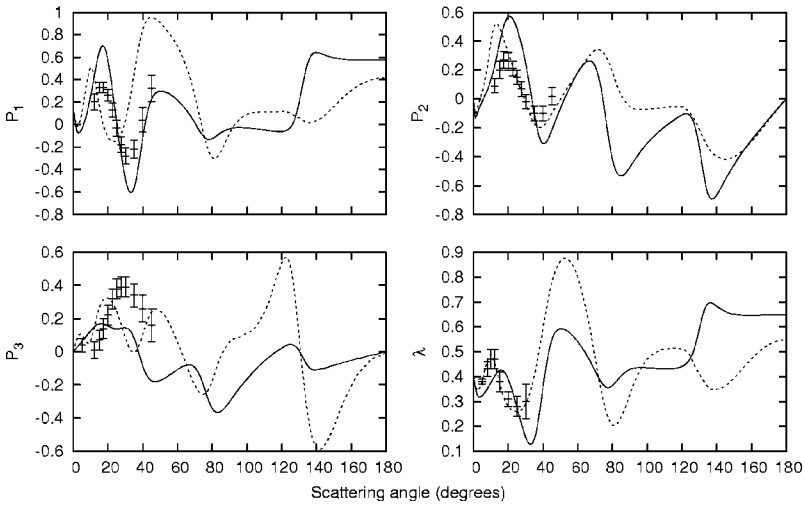

FIG. 13. Stokes parameters P_1, P_2, P_3, and λ values for the $6s5d\ ^1D_2$–$6s6p\ ^1P_1$ excitation in barium at 20 eV. The full curve represents the present RDW results. Data from [5] are dashed curve, 115-state CCC results; + with error bars, experimental measurements.

though there is some singlet-triplet mixing here it is quite minor since *LS* coupling becomes increasingly valid for the more highly excited states. Although the shapes of the PDCSs and DCSs are very similar, there is a noticeable difference in magnitude. In contrast, both the UDWA calculations and the experiment exhibit a strong forward peak characteristic of an allowed transition. If the smaller magnitude of the RDW DCS results is accurate for small scattering angles, this could indicate that the experimental measurements are contaminated from nearby allowed transition with a much larger DCS. As in the previous cases, the CCC results where they exist are in good agreement with the experimental data.

In anticipation of new measurements [17] we present cross sections for the excitation of the $6s6p\ ^1P_1$ state to the $6p5d\ ^1D_2$, $5d^2\ ^1D_2$, $6s7s\ ^1S_0$, and $6s7p\ ^1P_1$ states in Fig. 12 for electron-impact energies of 20 eV along with CCC and UDWA results. The first and last of these are forbidden (odd-odd) transitions while the other two are allowed. The cross sections in the forward direction are noticeably smaller for the forbidden transitions as compared to the allowed ones. There is fair agreement between the three theoretical results for the allowed transitions, especially in shape, but the agreement is less satisfactory for the forbidden transitions. It will be of interest to find the experimental results for these cases although if they are limited to smaller scattering angles as in the previously reported results, they will not be of much help in distinguishing between the various theoretical results.

B. Coherence parameters

Turning to the Stokes parameters for the $6s5d\ ^1D_2$–$6s6p\ ^1P_1$ transition we show the RDW and CCC results at 20 eV in Fig. 13 along with the experimental measurements of Johnson *et al.* [6]. We note that the Stokes parameter P_1 has a nonzero value for 0° scattering but is not unity, unlike scattering from a $^1S_0$ state (such as the ground state). For P_1 the RDW results agree well with the behavior of the experimental data but the magnitudes at the extrema are larger than the measured values. The maxima and minima of the CCC results are shifted in position from both the RDW and experimental results. In the case of P_2 the CCC calculations are in good agreement with experiment for scattering angles greater than 20° while the RDW curve is in better agreement at smaller angles. Both sets of theoretical data have similar behavior over the whole range of scattering angles. For P_3 neither of the theories agrees well with experiment or with each other. We also show the λ values in

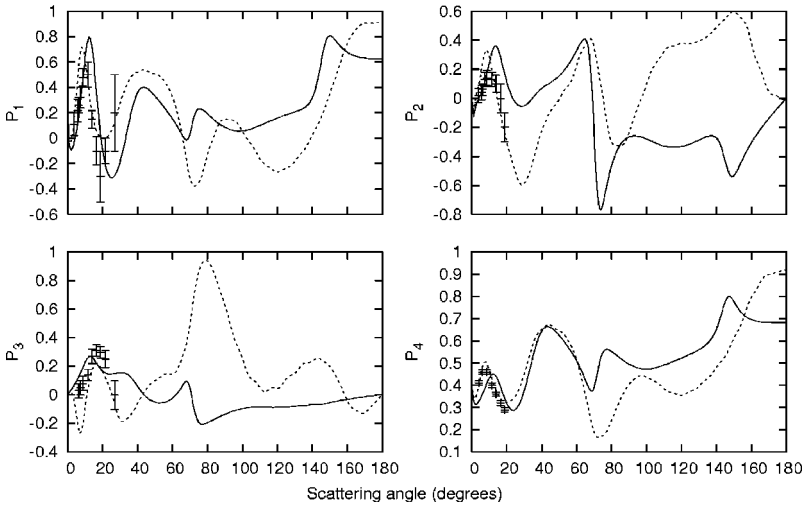

FIG. 14. As for Fig. 13 but at 40 eV.

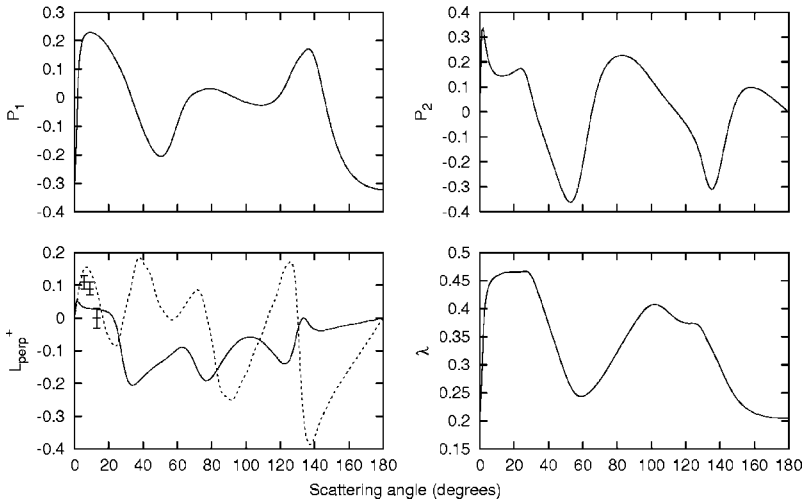

FIG. 15. Stokes parameters P_1, P_2, $L^+_{\text{perp}} = -P_3$, and λ values for the combined $5d6p\ ^1D_2$–$6s6p\ ^1P_1$ and $5d^2\ ^1D_2$–$6s6p\ ^1P_1$ deexcitation in barium at 20 eV. The full curve represents the present RDW results. Data from [7] are dashed curve, CCC results; + with error bars, experimental measurements.

this figure. Here the CCC results are in good agreement with experiment while the RDW extrema are somewhat shifted in position and magnitude.

Figure 14 shows the same results as Fig. 13 but for an incident energy of 40 eV. For P_1, P_2, and λ the RDW and CCC results are in closer agreement with each other at smaller scattering angles than at 20 eV while the agreement with experiment is very similar. For P_3 there is much better agreement between theory and experiment than at 20 eV. However, the CCC results show a pronounced minimum near 7° that does not appear in either the RDW calculations or the experiment. At larger scattering angles there is considerable variation in magnitude for all four EICPs.

Johnson *et al.* [7] have measured $L^+_{\text{perp}} = -P_3$ for features 1, 3, 6, 7, and 8 as listed in Table II at 20 eV incident electron energy. This paper also contains CCC calculations to compare with the measured quantities. They also presented CCC results which took into account the finite interaction volume of the experiments but since the difference was less than the experimental error bars we have not considered this. Since the other EICPs are also being measured for these transitions [17] we show our RDW results for the complete set in the following figures and compare with the experimental results and CCC calculations where available.

Figure 15 shows the results for feature 1, results from the deexcitation of the unresolved $5d6p\ ^1D_2$ and $5d^2\ ^1D_2$ levels to the $6s6p\ ^1P_1$ level. Since the deexcitation of the $5d6p\ ^1D_2$ level is an odd-odd parity transition and $J_a + J_b$ is odd, the direct scattering amplitude in the forward scattering is zero in a first-order theory such as the RDW and P_1 is very close to −1 here. Thus P_1 for the combined transition starts off with a negative value. For the L^+_{perp} parameter there is considerable difference between the RDW and CCC results. The experimental results lie below the CCC results but have a similar shape. Figure 16 presents the data for the $5d^2\ ^3P_2$ to $6s6p\ ^1P_1$ deexcitation. This is a dipole-allowed transition and P_1 starts off with positive values. For both the RDW and CCC calculations the L^+_{perp} values are almost identical with the ones for the $5d^2\ ^1D_2$ to $6s6p\ ^1P_1$ transition (not shown separately) although this is not the case for the other EICPs. Since the two $5d^2$ upper states are formed from the same configurations but have different energies and mixing coefficients this is not too surprising. Here the CCC results agree with experimental measurements within the error bars while the RDW results produce a similar shape but smaller magnitude at small scattering angles.

In Fig. 17 we show the EICPs for the $6s7s\ ^1S_0$ to $6s6p\ ^1P_1$ deexcitation. Note that this has the same level designation as

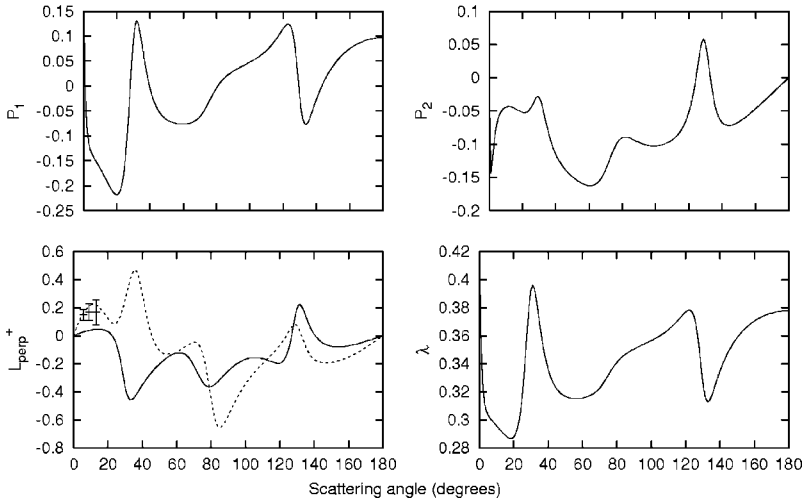

FIG. 16. As for Fig. 15 for the $5d^2\ ^3P_2$–$6s6p\ ^1P_1$ deexcitation.

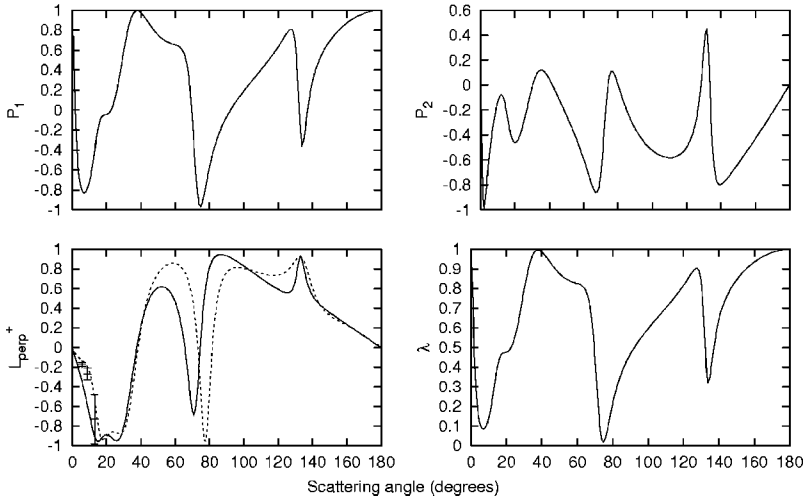

FIG. 17. As for Fig. 15 for the $6s7s\ ^1S_0$–$6s6p\ ^1P_1$ deexcitation.

the excitation from the ground $6s^2\ ^1S_0$ state to the $6s6p\ ^1P_1$ level. In fact, the P_1 parameter is very similar to that calculated by Srivastava *et al.* [8] at 40 eV. In particular, P_1 is unity for scattering at 0°. Here our $L^+_{\rm perp}$ values are quite similar to the CCC results and the experimental values lie between the two curves. The results for the deexcitation of the $6s7p\ ^1P_1$ level to the $6s6p\ ^1P_1$ level are shown in Fig. 18. This is an odd-odd parity transition and hence dipole forbidden but since J_a+J_b is even here the direct scattering amplitude is not zero for forward scattering and P_1 is positive there. The EICPs for this transition have rather different behavior from the others considered in this paper. The RDW and CCC results for $L^+_{\rm perp}$ are quite different here, the RDW results being close to zero at almost all scattering angles and in good agreement with experiment. Finally in Fig. 19 we show the results for the deexcitation of the $6s6d\ ^1D_2$ level. This transition is similar to the one shown in Fig. 13 and P_1 in particular is quite similar in these two cases. There is reasonable agreement between the RDW and CCC results for $L^+_{\rm perp}$ except at larger scattering angles. The experiment produces similar results which generally lie somewhat below the theoretical results but have a very similar behavior.

One rather striking feature is that P_1 and λ have a very similar shape over most of the angular range for all the transitions shown here except for the combined transitions shown in Fig. 15. This is not entirely surprising since for a completely coherent transition $P_1=2\lambda-1$ (Anderson *et al.* [14]). This relationship holds nearly exactly for the $6s7s\ ^1S_0$ to $6s6p\ ^1P_1$ deexcitation shown in Fig. 17. This transition is almost completely coherent since $P_1^2+P_2^2+P_3^2$ is very nearly equal to unity at all scattering angles and $P_1=1$ at 0° where P_2 and P_3 must be zero. However, all the other transitions are far from coherent since $P_1^2+P_2^2+P_3^2$ is much less than unity for almost all angles. Since the wave functions are linear combinations of a number of configurations, this behavior cannot be explained by a simple angular momentum recoupling argument (e.g., the fine-structure effect).

IV. CONCLUSIONS

We have applied the RDW method to the calculation of DCSs and EICPs for inelastic electron scattering from excited states in barium. In order to get a good description of the excited states, either relativistically or nonrelativistically, a number of electron configurations have to be included. Thus these states cannot be simply described in either *LS* or *j-j* coupling schemes.

In general, there is reasonable agreement between the RDW, CCC, and UDWA results for the DCSs. All of the DCS measurements have been taken for small scattering

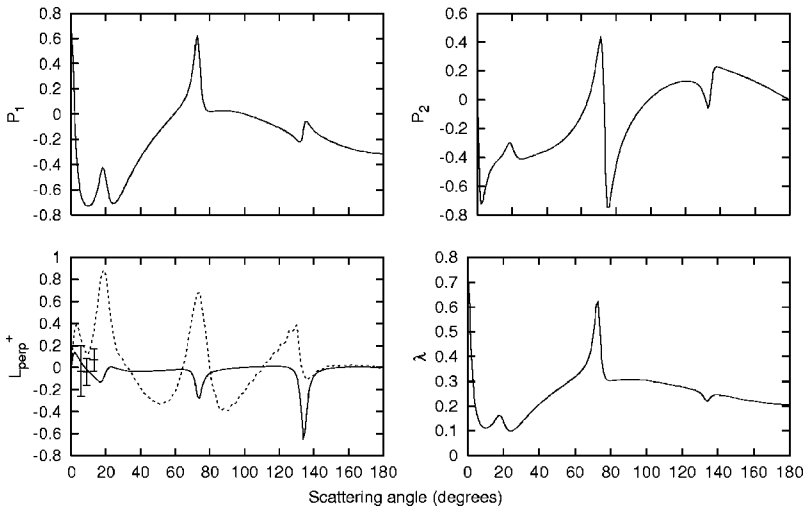

FIG. 18. As for Fig. 15 for the $6s7p\ ^1P_1$–$6s6p\ ^1P_1$ deexcitation.

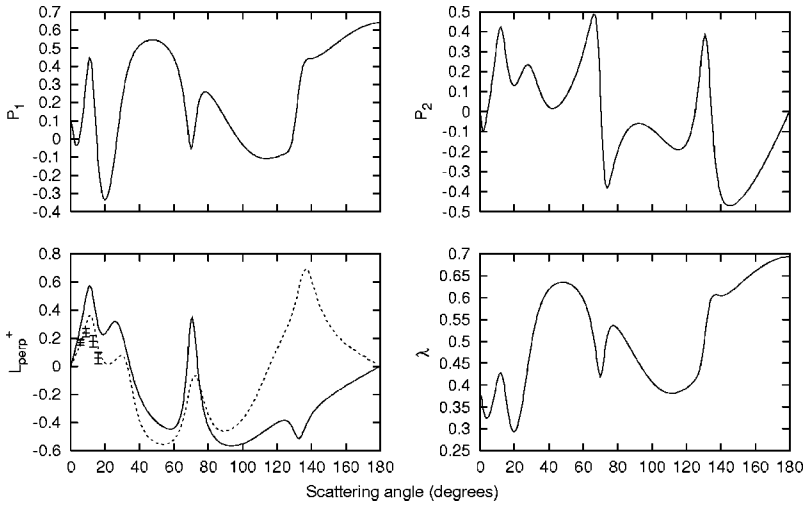

FIG. 19. As for Fig. 15 for the $6s6d\ ^1D_2$–$6s6p\ ^1P_1$ deexcitation.

angles where the cross sections are relatively large and they generally agree best with the CCC results. Measurements at larger angles would provide a more stringent test of the theories since the differences among the different theoretical results are larger for larger scattering angles. Unfortunately, the cross sections are substantially smaller there, making measurements extremely difficult.

In the case of the EICPs, there are no UDWA calculations and there are considerable differences between the RDW and CCC calculations in many cases. The experimental measurements do extend to larger scattering angles but only for a single transition. However, the agreement with the experimental data is somewhat inconsistent. We look forward to additional measurements for these parameters.

This study of electron scattering from excited states indicates that the strength of the RDW calculations lies in the calculation of the EICPs. UDWA results do not exist for these quantities and the agreement between the CCC results and experiment is less good than for the DCSs.

ACKNOWLEDGMENTS

We are grateful to George Csanak and Dimitry Fursa for sending their theoretical data in numerical form including previously unpublished results. This work was supported in part by a grant to A.D.S. from the Natural Sciences and Engineering Research Council of Canada. R.S. is thankful to the Council of Scientific and Industrial Research (CSIR) for financial support of this work.

[1] D. F. Register, S. Trajmar, S. W. Jensen, and R. T. Poe, Phys. Rev. Lett. **41**, 749 (1978).
[2] Y. Li and P. W. Zetner, J. Phys. B **28**, 5151 (1995).
[3] Y. Li and P. W. Zetner, J. Phys. B **29**, 1803 (1996).
[4] P. W. Zetner, S. Trajmar, S. Wang, I. Kanik, G. Csanak, R. E. H. Clark, J. Abdallah, Jr., and J. C. Nickel, J. Phys. B **30**, 5317 (1997).
[5] P. W. Zetner, S. Trajmar, I. Kanik, S. Wang, G. Csanak, R. E. H. Clark, J. Abdallah, Jr., D. Fursa, and I. Bray, J. Phys. B **32**, 5123 (1999).
[6] P. V. Johnson, B. Eves, P. W. Zetner, D. Fursa, and I. Bray, Phys. Rev. A **59**, 439 (1999).
[7] P. V. Johnson, P. W. Zetner, D. Fursa, and I. Bray, Phys. Rev. A **66**, 022707 (2002).
[8] R. Srivastava, T. Zuo, R. P. McEachran, and A. D. Stauffer, J. Phys. B **25**, 3709 (1992).
[9] K. Muktavat, R. Srivastava, and A. D. Stauffer, J. Phys. B **37**, 2165 (2004).
[10] F. A. Parpia, C. Froese Fischer, and I. P. Grant, Comput. Phys. Commun. **94**, 249 (1996).
[11] C. E. Moore, *Atomic Energy Levels*, Natl. Bur. Stand. (U.S.) Circ. No. 467 (U.S. GPO, Washington, D.C., 1958), Vol. III.
[12] H. Karlsson and U. Litzén, Phys. Scr. **60**, 321 (1999).
[13] T. Zuo, R. P. McEachran, and A. D. Stauffer, J. Phys. B **24**, 2853 (1991).
[14] N. Andersen, J. W. Gallagher, and I. V. Hertel, Phys. Rep. **165**, 1 (1988).
[15] J. Z. Klose, J. R. Fuhr, and W. L. Wiese, J. Phys. Chem. Ref. Data **31**, 217 (2002).
[16] D. Fursa (private communication).
[17] P. W. Zetner (private communication).